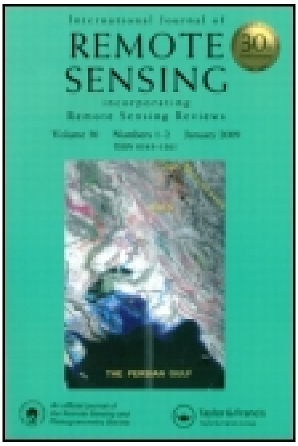

International Journal of Remote Sensing
Publication details, including instructions for authors and subscription information:
http://www.tandfonline.com/loi/tres20

Infrastructure assessment for disaster management using multi-sensor and multi-temporal remote sensing imagery

Matthias Butenuth [a], Daniel Frey [a], Allan Aasbjerg Nielsen [b] & Henning Skriver [b]

[a] Technische Universität München, Remote Sensing Technology, München, 80333, Germany

[b] Technical University of Denmark, National Space Institute, Lyngby, 2800, Denmark

Version of record first published: 28 Sep 2011.

To cite this article: Matthias Butenuth, Daniel Frey, Allan Aasbjerg Nielsen & Henning Skriver (2011): Infrastructure assessment for disaster management using multi-sensor and multi-temporal remote sensing imagery, International Journal of Remote Sensing, 32:23, 8575-8594

To link to this article: http://dx.doi.org/10.1080/01431161.2010.542204

International Journal of Remote Sensing
Vol. 32, No. 23, 10 December 2011, 8575–8594

Infrastructure assessment for disaster management using multi-sensor and multi-temporal remote sensing imagery

MATTHIAS BUTENUTH*†, DANIEL FREY†, ALLAN AASBJERG NIELSEN‡ and HENNING SKRIVER‡
†Technische Universität München, Remote Sensing Technology, München 80333, Germany
‡Technical University of Denmark, National Space Institute, Lyngby 2800, Denmark

(*Received 29 June 2010; in final form 18 October 2010*)

In this article, a new assessment system is presented to evaluate infrastructure objects such as roads after natural disasters in near-realtime. A particular aim is the exploitation of multi-sensor and multi-temporal imagery together with further geographic information system data in a comprehensive assessment framework. The combination is accomplished combining probabilities derived from the different data sets. The assessment system is applied to two different test scenarios evaluating roads after flooding, yielding very promising results and evaluation values concerning completeness and correctness. The benefit of the data combination, in particular the multi-temporal component, demonstrates the suitability of the proposed method for different application scenarios.

1. Introduction

In this article, a novel assessment system of infrastructure objects is presented using multi-sensor and multi-temporal imagery after natural disasters. The automatic and ongoing derivation of up-to-date information from imagery is of vital importance to support a fast disaster management after flooding, earthquakes or landslides (Chesnel *et al.* 2007, Rehor *et al.* 2008, Frey and Butenuth 2009). The focus of the introduced assessment system is on the development of strategies and methods to evaluate the status of infrastructure objects such as roads, in consideration of the crucial factor time as the dominating condition to support the fast reaction.

Great efforts have been made in order to speed up the workflow from data acquisition including satellite tracking up to the point of map generation (Voigt *et al.* 2007). Data analysis consisting of information extraction, damage assessment, thematic analysis and change detection plays a decisive role in the processing chain (Bamler *et al.* 2006). However, many data analysis tasks are currently done manually which is very time consuming and, thus, automation is required to substitute the manual interpretation. The difficulty is the development of methods minimizing wrong decisions to avoid fatal consequences in emergency actions.

The general process of providing remote-sensing information for disaster management can be divided into three parts: first, available satellites have to be selected and commanded immediately. Secondly, the acquired raw data have to be processed with specific signal processing algorithms to generate images suitable for interpretation,

*Corresponding author. Email: matthias.butenuth@bv.tum.de

International Journal of Remote Sensing
ISSN 0143-1161 print/ISSN 1366-5901 online © 2011 Taylor & Francis
http://www.tandf.co.uk/journals
http://dx.doi.org/10.1080/01431161.2010.542204

particularly for synthetic aperture radar (SAR) images. Thirdly, the interpretation of multi-sensor images so as to get geometrically precise and semantically correct information as well as the production of digital maps need to be conducted in the shortest possible time frames. While the first two aspects are mostly related to the optimization of processing chains and hardware capabilities, further research is needed concerning the third aspect: the fast, integrated and geometrically and semantically correct interpretation of multi-sensor and multi-temporal images.

The focus and novel contribution of this article is the combination of multi-sensor and multi-temporal components in a comprehensive assessment system. The combination is accomplished combining probabilities derived from the different input data. The integration of every kind of imagery in the system is an important prerequisite to guarantee a fast assessment independently of the available sensor type. In this article, a modular system is presented which is able to deal with varying data sources embedding all obtainable information to ensure the transferability of the developed strategy and methods. In addition, the integration of different imagery from different time points has several advantages compared to current solutions: multi-temporal images provide the opportunity to monitor a natural disaster chronologically during a period of time, not only at a specific time point. Moreover, the assessment of infrastructure objects at the time point t_2 can be improved using the results from time point t_1.

In §2 the state of the art regarding existing up-to-date damage assessment systems is presented and categorized in area- and object-based systems. In addition, data fusion techniques with regard to disaster management are discussed, and the basics of Gaussian mixture models and change detection methods are introduced since these methods are key elements of the assessment system. In §3 the new general assessment system is presented, which contains on a pixel level a supervised multi-spectral classification by means of Gaussian mixture models and belief functions derived from geographic information system (GIS) data. In §4 the system is applied to two different test scenarios using multi-sensor and multi-temporal imagery. The results shown are investigated and evaluated concerning their quality measures. Finally, further investigations and future work are pointed out in §5.

2. State of the art and basics

2.1 *Infrastructure assessment systems*

In the case of natural disasters it is reasonable to differentiate between object-based and area-based damage assessment systems. The focus of *object-based systems* is the assessment of infrastructural objects such as roads or buildings concerning their functionality. In recent years, several systems have been developed estimating the extent and type of destruction on various buildings. The damage assessment was realized using different kinds of sensors such as light detection and ranging (LIDAR; Rehor *et al.* 2008), SAR data (Gamba *et al.* 2007) and high-resolution spaceborne (Chesnel *et al.* 2007) and airborne images (Guo *et al.* 2009). However, most methods focus on only one single sensor and, thus, the adaptability is limited depending on the availability of data sources after a natural hazard. There are few approaches which analyse the possible advantages of combining different sensors for damage detection (Stramondo *et al.* 2006). The evaluation of individual objects such as damaged bridges is investigated using high-resolution SAR images (Balz *et al.* 2009). Even though bridges are crucial bottlenecks in the transportation systems, in the case of natural hazards a comprehensive assessment system of the whole road network is necessary. Further research developing automatic methods to assess transportation lifelines after natural disasters is important (Morain and Kraft 2003). Research dealing with the quality assessment of road databases has been carried out by Gerke and Heipke (2008), but the underlying strategy and model is based on an operational road network, not affected by natural hazards. In Frey and Butenuth (2009) a near-realtime assessment system of a road network using GIS objects and multi-sensor data is presented, but a multi-temporal component is not included into the system. The road objects are classified into different states using the ample paradigm proposed by Förstner (1996).

On the other hand, *area-based systems* focus on affected regions. Typical examples are the generation of flood masks derived from different sensors. Besides optical imagery, SAR data in particular are suitable for the extraction of inundated areas. A split-based automatic thresholding method to detect flooded areas from TerraSAR-X data in near-realtime is used by Martinis *et al.* (2009). A further semi-automatic approach using TerraSAR-X data is proposed in the work of Mason *et al.* (2010) detecting flooded regions in urban areas. The authors point out that in urban areas in particular the quality of the results is limited due to the side-looking principle of the radar sensor.

2.2 *Data fusion*

In general, the performance of damage assessment systems can be improved by including additional imagery and data sources. In particular, the combination of optical and radar images leads to an improved damage assessment (Stramondo *et al.* 2006). The system presented in this article is designed in a flexible way such that the benefits of data fusion can be completely exploited, but it is not dependent on specific sensors. This adaptability to different case scenarios distinguishes the presented approach from the previous methods mentioned above. The additional benefit depends on the way data are combined. Pohl and Van Genderen (1998) differentiate between three different levels of image fusion: pixel level, feature level and decision level. A review of the latest research of multi-source data fusion is given in Zhang (2010), who updates these three levels of data fusion with current developments pointing to the importance of high-level fusion approaches which include feature-level and decision-level fusion. For the assessment of infrastructural objects high-level data fusion is of utmost importance, because conclusions of the status of objects are needed. The combination of different data sources, for example, vector and image data, is discussed in several other contributions to emphasize the benefit, for example, Butenuth *et al.* (2007). In particular, the integration of GIS information combined with imagery improves the results and simplifies the decision making enormously (Brivio *et al.* 2002). A method for mapping the floodplain combining optical imagery and digital elevation model (DEM) is presented in Wang *et al.* (2002). For each data source an individual flood mask is generated, so that the final flood mask consists of the set union of the individual masks. Considering the DEM as an image, this approach belongs to the decision-level image fusion as defined in Pohl and Van Genderen (1998). The approach presented in this article combines imagery and DEM, too, to detect flooded areas. In contrast to the approaches discussed above, the aim is the combination based on probabilities derived from the input data.

2.3 *Change detection: multivariate alteration detection*

Change detection algorithms are widely used to investigate the extent and damage of natural disasters. A comprehensive review on change detection methods is given, for example, in Lu *et al.* (2004) and Coppin *et al.* (2004). However, many methods are restricted to specific sensor characteristics. The efficient response in the case of natural disasters requires a change detection method which is able to deal with various sensors containing a different number of channels. Furthermore, the influence of changing atmospheric conditions should be minimized. The multivariate alteration detection (MAD) method is invariant to linear transformation, which implies an insensitivity to linear atmospheric conditions or sensor calibrations at two different times (Nielsen *et al.* 1998).

The MAD transformation is based on canonical correlation analysis (CCA) which was originally introduced by Hotelling (1936). Unlike principal component analysis (PCA) which identifies patterns of relationships within one set of data, CCA investigates the intercorrelation between two sets of variables. Let $\boldsymbol{F} = \{F_1, F_2, \dots, F_n\}$ and $\boldsymbol{G} = \{G_1, G_2, \dots, G_m\}$ be two images with n or m channels ($n \leq m$). A linear combination of the intensities for all channels leads to the transformed images U and V:

$$\begin{aligned} U &= \vec{\mathbf{a}}\boldsymbol{F} = a_1F_1 + a_2F_2 + \ldots + a_nF_n, \\ V &= \vec{\mathbf{b}}\boldsymbol{G} = b_1G_1 + b_2G_2 + \ldots + b_mG_m. \end{aligned} \tag{1}$$

The goal of the transformation is to choose the linear coefficient $\vec{\mathbf{a}}$ and $\vec{\mathbf{b}}$ minimizing the correlation between U and V. This leads to the result that the difference image between the transformed images U and V will have a maximum variance. Multiples of U and V would have the same correlation, which is why a reasonable constraint $\mathrm{var}(U) = 1$ and $\mathrm{var}(V) = 1$ is chosen:

$$\mathrm{var}(U - V) = \mathrm{var}(U) + \mathrm{var}(V) - 2\mathrm{cov}(U, V) = 2(1 - \mathrm{cov}(U, V)). \tag{2}$$

Using CCA, the linear coefficients $\vec{\mathbf{a}}$ and $\vec{\mathbf{b}}$ are determined and the MAD variates M_i can be calculated (Nielsen *et al.* 1998):

$$M_i = U_i - V_i \quad \text{for } i = 1, \ldots, n. \tag{3}$$

An extension to the MAD transformation is the iteratively reweighted MAD (IRMAD) method. Similar to boosting methods in data mining, an iteration schema focuses on observations whose change status are uncertain (Nielsen 2007). Since the MAD or IRMAD variates can only be interpreted in a statistical manner there is a need to assign a semantic meaning to the MAD variates. In Canty and Nielsen (2006) an unsupervised classification method is proposed based on the MAD variates to cluster pixels in no-change and one or more change categories.

2.4 *Combination of probability functions: Gaussian mixture model*

The radiometric characteristics of infrastructural objects of the same type could vary strongly, which is why single probability functions are not able to describe the complex scenes sufficiently. Therefore, mixture models are used which combine single functions into a more complex probability function. The resulting probability function $p(\boldsymbol{y}|\theta)$ is simply a weighted sum of the initial functions $p_j(\boldsymbol{y}|\theta_j)$:

$$p(\boldsymbol{y}|\theta) = \sum_{j=1}^{k} \alpha_j p_j(\boldsymbol{y}|\theta_j). \tag{4}$$

Each θ_j describes the set of parameters defining the jth component, $\alpha_1, \ldots, \alpha_j$ are the weights called the mixing probabilities and $\boldsymbol{y} = [y_1, \ldots, y_d]^\top$ represents one particular outcome of a d-dimensional random variable $\boldsymbol{Y} = [Y_1, \ldots, Y_d]^\top$. Often Gaussians are used for $p_j(\boldsymbol{y}|\theta_j)$. The mixing probabilities have to fulfill the following equations:

$$\alpha_j \geq 0,\ j = 1, \ldots, k \text{ and } \sum_{j=1}^{k} \alpha_j = 1. \tag{5}$$

The expectation maximization (EM) algorithm is used to determine α_j and θ_j. A detailed description of mixture models can be found in McLachlan and Peel (2000). The number of centres j is calculated using the minimum message length (MML) criterion (Wallace 2005). The detailed algorithm of MML is described in Figueiredo and Jain (2002). Different mixture models, especially for SAR images where the data is generally non-Gaussian, have been described in Bouguila and Ziou (2006) using finite Dirichlet mixture models and in Ziou *et al.* (2009) using finite Gamma mixture models.

3. Assessment system

3.1 *System*

The assessment system has a modular and very flexible structure to cope with varying raw data being available in emergency cases (see figure 1). Nevertheless, there are some prerequisites to applying the system. The GIS objects which should be evaluated concerning their functionality must be given. It is conceivable to extract the GIS objects using imagery before the natural disaster takes place or, alternatively, from a GIS. However, in view of the performance of automatic extraction methods, objects from a given GIS database with a guaranteed quality concerning correctness and completeness are better suited. The result of the assessed GIS objects depends strongly on the available input information. Besides the imagery, DEM and further GIS information can be embedded into the system. Here, this data is called *input data*.

A supervised multispectral classification is accomplished on a pixel level by means of Gaussian mixture models (GMMs) to interpret the multi-spectral imagery. The mixing coefficients for the Gaussian mixtures are determined from the EM algorithm. Belief functions are introduced to derive probabilities from GIS information to be exploited during the assessment. If multi-temporal images are available change detection methods such as the MAD algorithm are used to derive probabilities of change between different time points. The combination of the different input data is carried out in the probability level. All individual methods regarding specific input data and the combination of the derived probabilities are realized at a pixel level. In contrast, the subsequent assignment of GIS objects to the states *intact, possibly intact* or *not intact/destroyed* using maximum likelihood estimation is object-based (see figure 1).

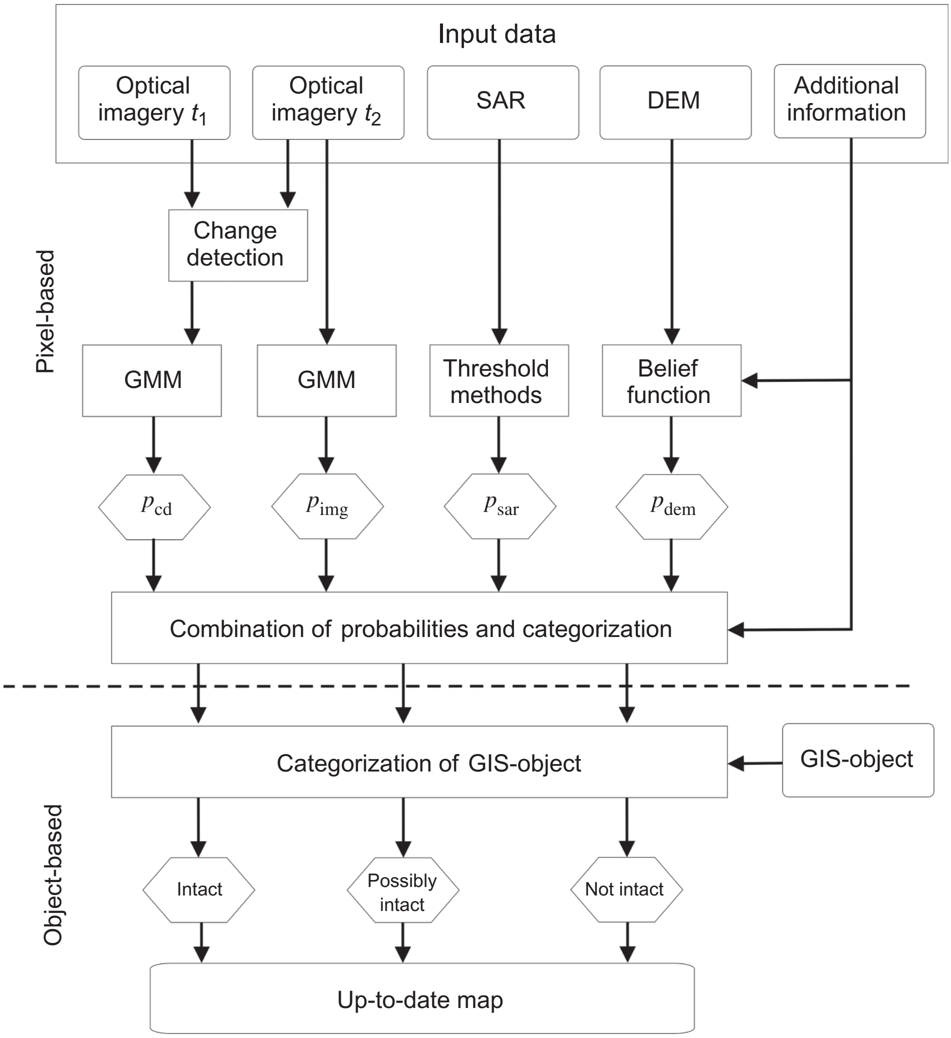

Figure 1. General damage assessment system.

3.2 *Methods and combination of probabilities*

For each input data individual methods have to be applied to derive individual probabilities evaluating infrastructural objects (see figure 1). Given multi-spectral imagery as input data, a multi-spectral classification is carried out. The infrastructural objects are classified to different classes relating to the states *intact, possibly intact* and *not intact/destroyed*. Since many classes such as roads have no consistent radiometric characteristic as shown in figures 2 and 3, the probability density function which is needed to describe the class road is more complex than a multivariate Gaussian distribution. Therefore, the GMM is used to calculate the more complex probability density function by summing up several multivariate Gaussian distributions. The parameters for the individual Gaussian distributions are derived using the EM algorithm. This approach is applied to every class, but a real benefit of the GMM compared to a single Gaussian distribution is only noticeable in the case of the class road due to the different

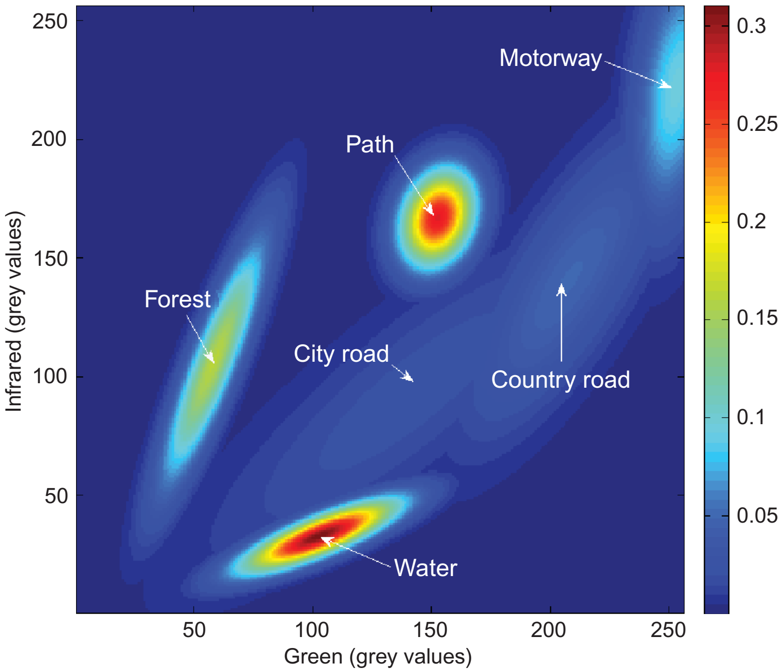

Figure 2. Two-dimensional probability density functions of the classes forest and water and the separated road classes (city road, country road, path and motorway). Exemplarily visualized using the infrared and green channel.

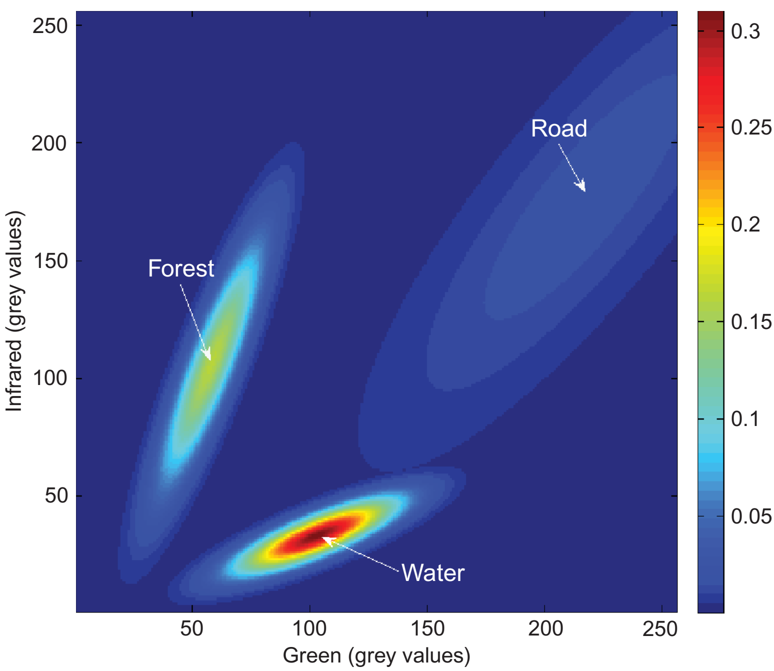

Figure 3. Two-dimensional probability density functions of the classes forest and water and a combined class road. Exemplarily visualized using the infrared and green channel.

radiometric characteristics. The resulting probabilities from the mixture model p_{img} are combined with probabilities from further input data (see figure 1). In the case of the assessment of roads concerning the trafficability after flooding, p_{img} represents the probability that a road segment belongs to the class water or road derived from the corresponding multivariate probability density functions generated from training samples. A road segment is derived from the available GIS data and can be defined with a specific length. The object-based probabilities are computed by a mean value of the related pixel-based probabilities.

The availability of images at different time points enables the utilization of change detection methods exploiting additional assessment criteria. The IRMAD algorithm enables the detection of changes and resulting IRMAD variates are classified using a supervised multispectral classification. For the different change states, that is, *intact* → *destroyed,* probability functions are generated. These probabilities p_{mad} are embedded into the assessment system. In figure 4(*c*) three IRMAD variates are shown as an RGB-colour image obtained from IKONOS images at time t_1, see figure 4(*a*), and time t_2, see figure 4(*b*). In this example of a flood event, the changed areas from flooded to not flooded are depicted in pink, the grey colour represents no change, see figure 4(*c*).

Additional GIS information such as DEM is often available offering the opportunity to enhance the assessment system. Since the combination of the input data is based on the probability level, probabilities also have to be derived from the GIS information. Belief functions can be generated depending on the GIS information. In figure 5 an example is shown which depicts the probability that an object is flooded depending on the elevation. The general probabilities p_{gis} can be modelled as belief functions. In the case of the assessment of flooded roads, the probabilities p_{dem} can be derived from the DEM in figure 5, that is, $p_{\mathrm{gis}} = p_{\mathrm{dem}}$.

The combination of the probabilities derived from the different input data is defined as following:

$$\begin{aligned} p_1 &= p_{1,\mathrm{img}} \cdot p_{1,\mathrm{gis}} \cdot \ldots \cdot p_{1,\mathrm{mad}} \\ p_2 &= p_{2,\mathrm{img}} \cdot p_{2,\mathrm{gis}} \cdot \ldots \cdot p_{2,\mathrm{mad}} \\ &\;\;\vdots \\ p_s &= p_{s,\mathrm{img}} \cdot p_{s,\mathrm{gis}} \cdot \ldots \cdot p_{s,\mathrm{mad}}. \end{aligned} \tag{6}$$

The probabilities p_i are the combined probabilities of one status i. In the easiest case, the set of states could be *intact* or *not intact*, but it is also reasonable to think of s different kinds of destruction states. Finally, the object is categorized into the state i with the highest probability. The probabilities p_{img} and p_{gis} are statistically independent. As part of the model, the statistical independence between p_{img} and p_{mad} can be assumed, because p_{mad} contains new information derived from the newly introduced image at time t_2.

3.3 *Workflow of rule-based classification*

Natural disasters can be divided into specific phases. In general, all disasters consist of three main time phases: pre-disaster, the disaster itself or maximum extent of disaster and post-disaster. Depending on the type of natural disaster the time phases can be further subdivided. The workflow of the rule-based classification system is dependent on the available imagery at different time points. In addition, the

(*a*)
(*b*)
(*c*)

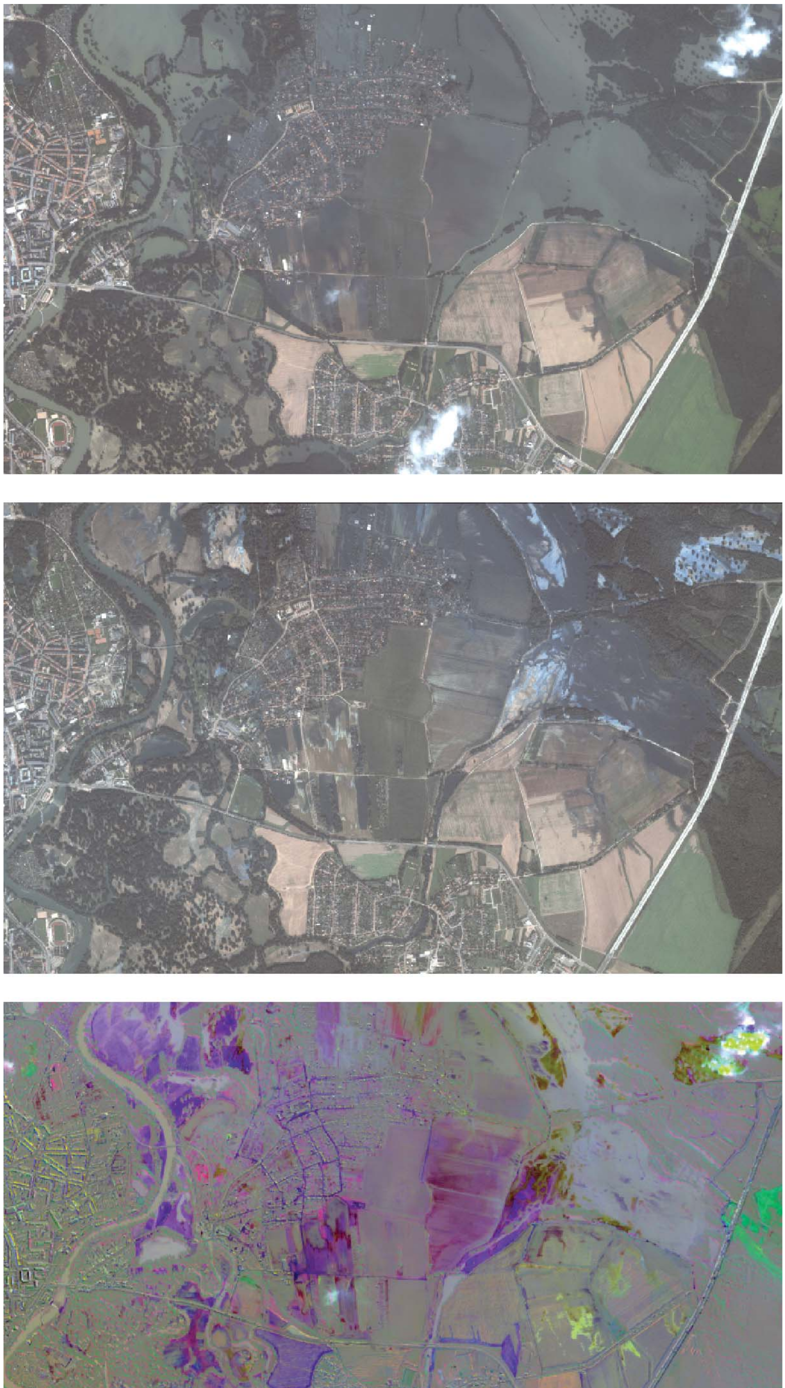

Figure 4. Change detection using the MAD algorithm: the IKONOS scene of the flooded area of the Elbe near Dessau, Germany, at time t_1 (*a*); the IKONOS scene of the flooded area at time t_2 (*b*); three MAD variates depicted as an RGB-colour image (*c*).

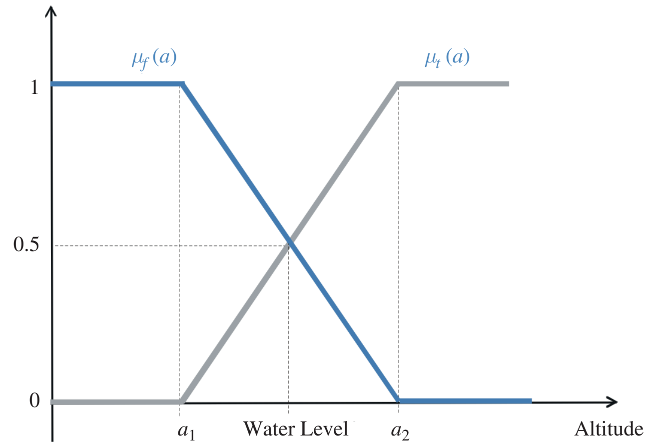

Figure 5. Belief functions depending on altitude: area is flooded (blue), area is not flooded (grey).

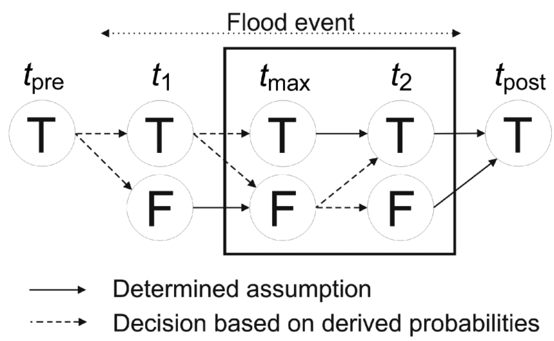

Figure 6. Possible development of the trafficability of roads during a flood subdivided into different time phases (T, trafficable; F, flooded).

type of natural disaster and the kind of infrastructural objects to be assessed lead to specific assumptions which can be embedded as rules in the classification system. In figure 6 an example of specific time points of a flooding event is shown which is important in order to carry out an analysis of, for example roads concerning their trafficability.

In the case of flooding it is reasonable to determine five time phases in which imagery can be acquired. All kinds of imagery being acquired before the natural disaster are assigned to the first time phase t_{pre}. During a flooding two different time phases can be subdivided: the water level increases t_1 until the water level reaches the maximum and the water level decreases t_2. In the following the time point between t_1 and t_2 is noted as t_{max}. In the model we assume that the water level at the time point t_{max} is higher than at the time point t_1 and t_2. The index 'max' stands not for the maximum water level during a flood but for the time point of the acquisition of an image. Imagery acquired after the flooding is noted as t_{post}. Depending on the time points when the images are acquired, different assumptions can be made leading to rules which are embedded into the classification system. For example, if two images at the time point t_1 and t_{max} are available it is reasonable to assume that roads which were flooded at time point t_1 are still flooded at time point t_{max}. This kind of assumption is depicted in figure 6 as a continuous arrow. In particular, if the information content of the image at time point t_1 is higher than at time point t_{max}, this additional assumption could improve the results at time point t_{max}. The circles illustrate the status of a road which can be trafficable T or flooded F. The dashed lines show the possible changes of the status of a road based on decisions derived from computed probabilities.

Similar graphs can be developed for different kinds of disasters and other infrastructural objects. In a semi-automatic approach it is imaginable that a manually generated categorization at a previous time point is used for the improved categorization at the current time point. Despite the time-consuming generation of the categorization there is no loss of time for the emergency response since the categorization at the previous time point can be done in advance before the current time point provides new remote sensing information. The improvement of this semiautomatic approach is shown in the test scenarios.

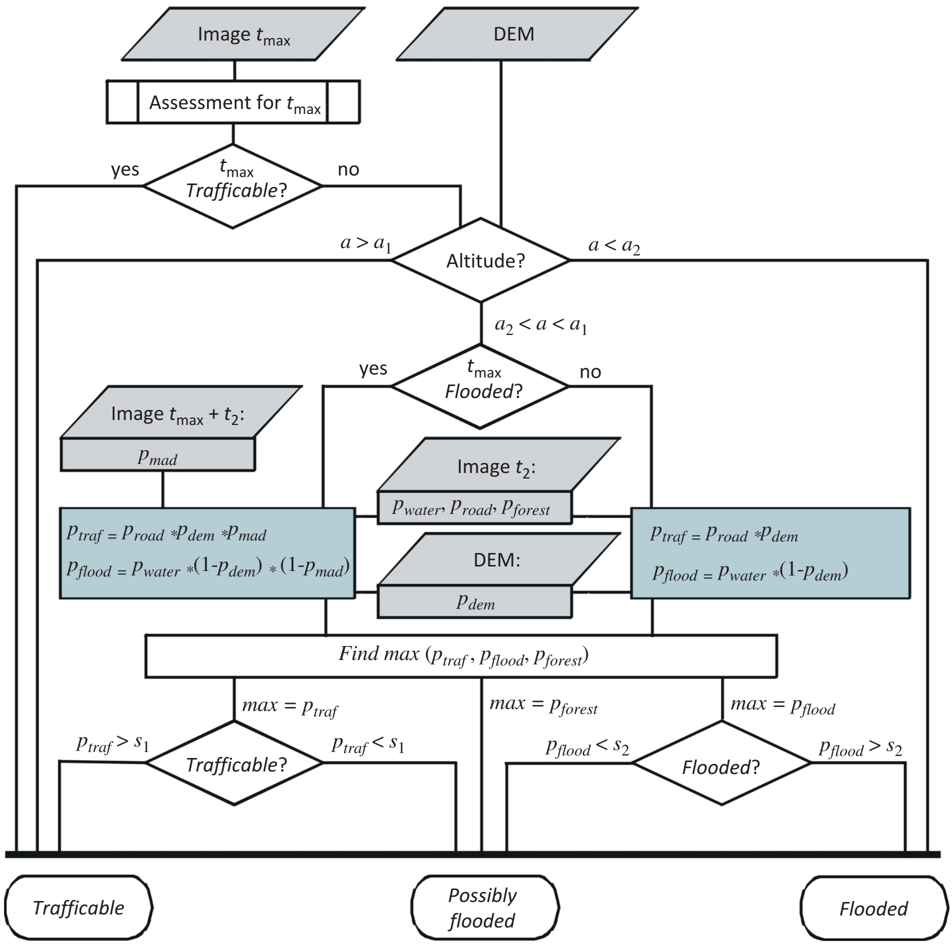

Figure 7. Example of workflow of rule-based classification describing the rectangular part of figure 6.

A detailed workflow of the rule-based assessment system is exemplarily depicted in figure 7 assuming the water level is decreasing (see figure 6, black rectangle). The input data are illustrated by the grey parallelograms (figure 7). Below these parallelograms the derived probabilities from the input data are attached in grey rectangles. The combination of the probabilities is realized in the blue boxes. The assessed road segments at time $t_{\max}$ and additional information such as the water level lead to the rule-based framework built on the combination of the probabilities. The probability p_{img} derived from the imagery at time point t_2 is partitioned into three different probabilities belonging to a specific class: water p_{water}, road p_{road} and forest p_{forest}. The classes road, water and forest are chosen, because only these classes are relevant for the object of interest (road) or its possible occurring occlusions (water, forest). The classification is only accomplished for the possible road areas, not for the whole image. Using a maximum likelihood estimation followed by a threshold operation the segment is categorized into the three states *trafficable*, *possibly flooded* and *flooded*.

4. Results and analysis

The damage assessment system presented is applied to two different flooding scenarios. In real case scenarios the availability of input data is the crucial factor. The derivation of the probabilities given in equation (6) is not always possible depending on the available data. On the other hand, often further information exists which is useful to generate additional rules. The combination of probabilities is embedded into a rule-based framework which can differ from case to case. In the following two scenarios road objects given from a GIS database are assessed concerning their trafficability.

4.1 *Test scenario Elbe (Germany)*

The first test scenario is the flooding of the river Elbe (Germany) in the year 2002. The available input data for the damage assessment system consists of two IKONOS scenes acquired on the 21 and 26 August, see figure 4(*a*) and figure 4(*b*). In addition, a DEM is available with a 10×10 m grid with a geometric accuracy of $+/-$ 1 m. The peak of the water level was measured on 19 August. The scene at the time point $t_{\max}$ shows almost the maximum inundated area. In the second scene at time t_2 the flooding receded strongly and only a small area is covered by water, see figure 4(*b*), top right.

The results obtained are compared to a manually generated reference. The information for the generation of the reference is only given in the image at time t_2. Therefore, it is not a comparison with the real ground truth, but it is the comparison of the automatic approach with the manual interpretation of a human operator. The reference is categorized into three different states: *trafficable*, *possibly flooded* and *flooded*. Since the categorization of the automatic system consists of the same states the following four different assignment criteria are determined: ‘correct assignment’, ‘manual control necessary’, ‘possibly correct assignment’ and ‘wrong assignment’. The ‘correct assignment’ indicates that the manually generated reference is identical with the result of the automatic system. In the case of ‘manual control necessary’ the automatic approach leads to the state *possibly flooded* whereas the manual classification assigns the line segments to *flooded* or *trafficable*. The other way around denotes the expression ‘possibly correct assignment’. The expression ‘wrong assignment’ indicates that one result categorizes the segment to *flooded* and the other to *trafficable*. The results

Table 1. Results and evaluation of the assessment system evaluating the road data of the test scenario Elbe exploiting different input data.

	t_2 (%)	t_2, DEM (%)	$t_{\max,2}$, DEM (%)	$t_{\max,2,c}$, DEM (%)
Correct	68.40	68.45	69.60	87.14
Manual	27.88	27.77	27.48	10.96
Possibly	2.64	2.72	2.52	1.79
Wrong	1.08	1.06	0.40	0.11

and evaluation of the combined interpretation of the enhanced automatic system are shown in table 1. All results are generated using GMMs.

The first column in table 1 represents the result using only the image t_2 without any further information. The result with about 1% 'wrong assignments' and about 68% 'correct assignment' is almost the same if an additional DEM is used, see table 1 (t_2, DEM). The reason for the lack of improvement could be ascribed to the low accuracy of the DEM used. The evaluated road segments are depicted in figure 8(*a*). Green road segments correspond to 'correct assignment', yellow to 'manual control necessary', cyan to 'possibly correct assignment' and red or blue belongs to 'wrong assignment'. If the system assigns a road segment to the state *trafficable* but the reference is *flooded* the road segment is coloured in red. Blue road segments are assigned to *flooded* by the system and *trafficable* by the reference.

In figure 8(*b*) the related result of the third column of table 1 is visualized which includes the additional scene at time point $t_{\max}$ as input data. The additional scene and the resultant calculated probability p_{mad} derived from the described MAD method leads to an improvement of the results. Several wrongly assigned segments disappear whereas the 'correct assignments', the assignments 'manual control necessary' and the 'possibly correct assignments' remain almost constant.

In figure 8(*c*) the results exploiting an additional manually generated reference from the previous scene $t_{\max}$ are plotted. The exploitation of the derived results from the previous time point as additional input information is reasonable, because the correct states of the objects at time point $t_{\max}$ can give hints to the evaluation of the current assessment at time point t_2. The numerical evaluation is presented in the fourth column of table 1 ($t_{\max,2,c,}$ DEM). The results are better by far than the previous results obtained. The 'correct assignments' arise from 69% to 87% and the 'wrong assignments' decrease from 0.4% to 0.1%. It is important to point out that a correct reference at the time point $t_{\max}$ has to be generated. Nevertheless, there is no influence to the near-realtime requirement of the system since the time consuming generation of the reference can be done before the current assessment at time point t_2.

The final result using the described assessment system is depicted in figure 9. All road segments are divided into four different states: besides the already mentioned states *trafficable* (green), *possibly flooded* (yellow) and *flooded* (red) an additional state *flooded* → *trafficable* (blue) is introduced by means of the change detection algorithm. This additional state is very useful for rescue teams since it shows the areas which are again trafficable after flooding.

4.2 *Test scenario Chobe river (Namibia)*

The second test scenario investigates the flooding that took place in the north of Namibia in March 2009. The used remote-sensing data consists of a SPOT image,

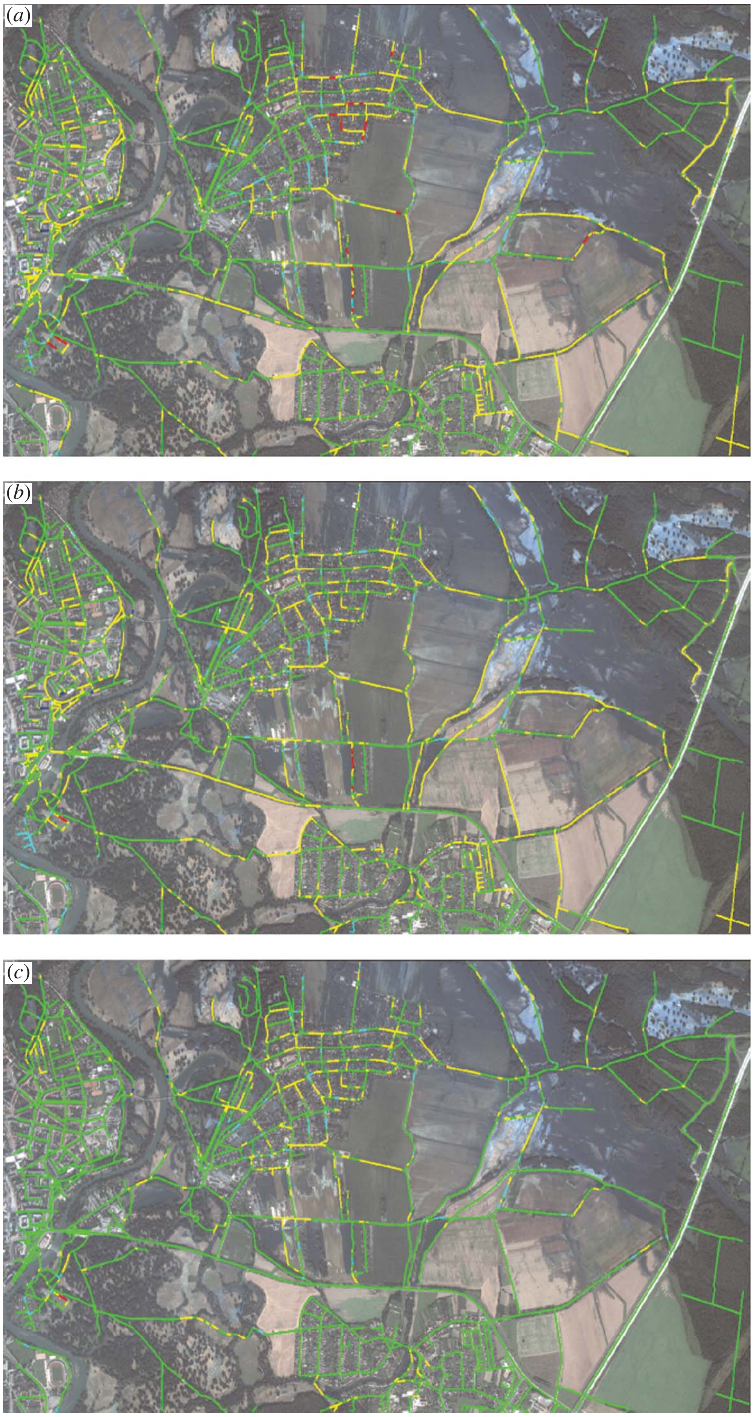

Figure 8. Evaluation of the assessment system (Elbe scenario) evaluation using image t_2 and DEM (*a*); evaluation using image t_2, image t_1 and DEM (*b*); detail of evaluation using image t_2, image t_1 with correctly assessed roads and DEM (*c*); green = 'correct assignment', yellow = 'manual control necessary', cyan = 'possibly correct assignment', red = 'wrong assignment' (system = *trafficable*, reference = *flooded*), dark blue = 'wrong assignment' (system = *flooded*, reference = *trafficable*).

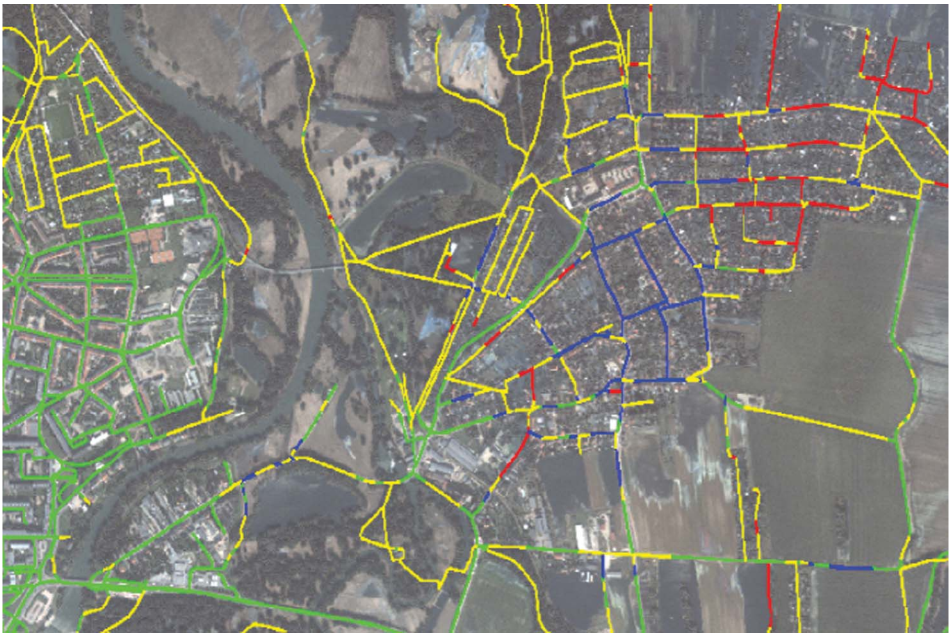

Figure 9. Detailed result of the assessment system using all available input data (Elbe scenario): image t_1, image t_2, DEM and manual generated reference at time t_1; green = *trafficable*, yellow = *possibly flooded*, red = *flooded*, dark blue = *trafficable* (change: *flooded* → *trafficable*).

acquired on 30 March with a resolution of 2.5 m, and a RapidEye image acquired on 8 April with a resolution of 6.5 m. The water level rises until 29 March and then increases slightly between 30 March and 8 April to the maximum. In the assessment system all available channels are used. In the case of the SPOT image three channels (red, green and infrared) and in the case of the RapidEye image five channels (red, green, blue, red edge and near-infrared) are available. Besides the image information a road network was extracted manually from a high-resolution Quickbird scene. The goal of this test scenario is again the assessment of the roads into three different states: *trafficable*, *possibly flooded* and *flooded*. In addition, an ASTER DEM was used with a spatial resolution of 15 m.

A reference was generated manually which classifies the roads into *trafficable* and *flooded* in order to evaluate the results of the assessment system. In contrast to the first test scenario no state *possibly flooded* is used in the reference leading to the three different assignment criteria: 'correct assignment', 'manual control necessary' and 'wrong assignment'.

In table 2 the results are shown using the image information from one image only. In both cases a Gaussian mixture model is applied and the DEM is used as additional information. The assessment of roads using the RapidEye image is significantly better than that using the SPOT image in spite of the worse resolution. Hence in this example the availability of radiometric information is more important than high resolution. This behaviour occurs due to the disregard of geometric information in the assessment system. In future work geometric features should also be embedded into the system.

Table 2. Results and evaluation of the assessment system evaluating the road data of the test scenario Chobe river exploiting different satellite images.

	SPOT (%)	RapidEye (%)
Correct	71.82	77.68
Manual	27.17	21.33
Wrong	1.01	0.99

Table 3. Results and evaluation of the assessment system evaluating the road data of the test scenario Chobe river exploiting different input data.

	$t_{\max}$ (%)	$t_{\max}$,GMM (%)	$t_{\max}$, DEM (%)	$t_{1,\max}$, DEM (%)	$t_{1,\max,c}$, DEM (%)
Correct	66.13	76.78	77.68	78.76	88.42
Manual	32.88	22.21	21.33	20.23	10.59
Wrong	0.99	1.01	0.99	1.01	0.99

In table 3 the improvement of the assessment system can be recognized, if additional data is included. The first and second columns show the results if only the image data at a time point $t_{\max}$ is used. In this test scenario the RapidEye scene is acquired at $t_{\max}$. The distinction between $t_{\max}$ and $t_{\max}$,GMM shows the difference using a GMM instead of a simple multivariate Gaussian distribution. The large improvement by using a mixture model can be traced back to the fact that the class road does not have consistent radiometric characteristics. Therefore, it is convenient to model the different subclasses of roads by a mixture model. The results of all further columns are gained using the GMM in order to build up the probability distributions. In column 3 the additional DEM information is embedded. The small improvement of the results can be partly ascribed to the bad resolution of the DEM. Unfortunately, a DEM with higher resolution was not available in order to investigate the influence of the accuracy of the DEM. The last two columns represent the results using in addition the image at time point t_1, which reflects in the test scenario the SPOT scene. The usage of the MAD algorithm and the automatically assessed roads at time point t_1 entails further improvements of the result as presented in the fourth column. In real applications it is also possible to generate a manually generated assessment of the roads at time point t_1. In the fifth column the result is shown if manually assessed roads at time point t_1 are available.

In figure 10 the graphical evaluation of the fourth column of table 3 is shown. The 'wrong assignments' depicted in red and blue (see figure 10) can be referred to different circumstances. Mainly all wrongly classified roads are located in the transition zone between flooded and non-flooded regions. The reasons for the misclassifications could be partly inundated roads, geometrical inaccuracies or even some errors in the manually generated reference. Figure 11 shows the final result consisting of the same states as already described in figure 9. Depending on the application the percentage of the 'wrong assignment' can be shifted using different parameter settings. In figure 12 the assignments are depicted depending on the parameter s_1. By means of the threshold parameter s_1 the road object is categorized to the states *trafficable* or *possibly flooded* (see figure 7). As it is depicted in figure 12 the results of the system

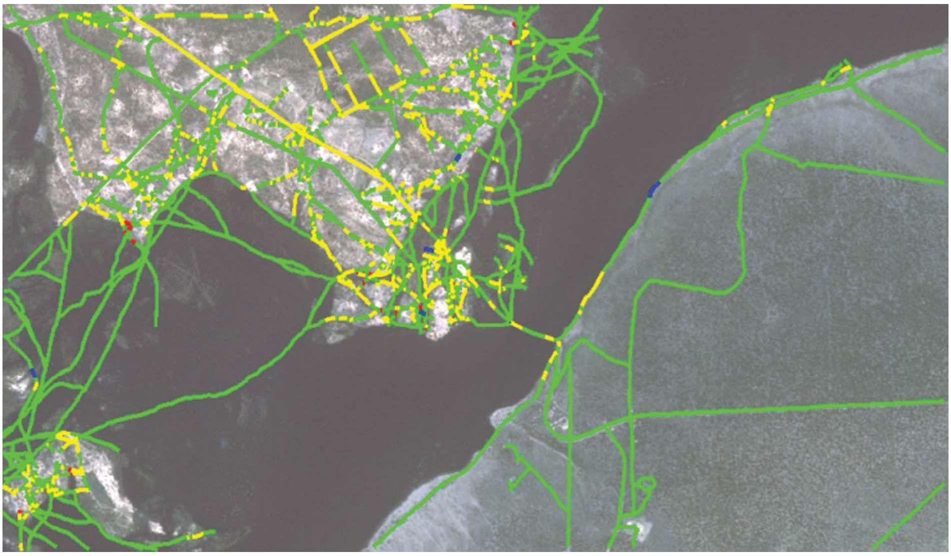

Figure 10. Evaluation of the assessment system (Chobe scenario) green = 'correct assignment', yellow = 'manual control necessary', red = 'wrong assignment' (system = *trafficable*, reference = *flooded*), dark blue = 'wrong assignment' (system = *flooded*, reference = *trafficable*).

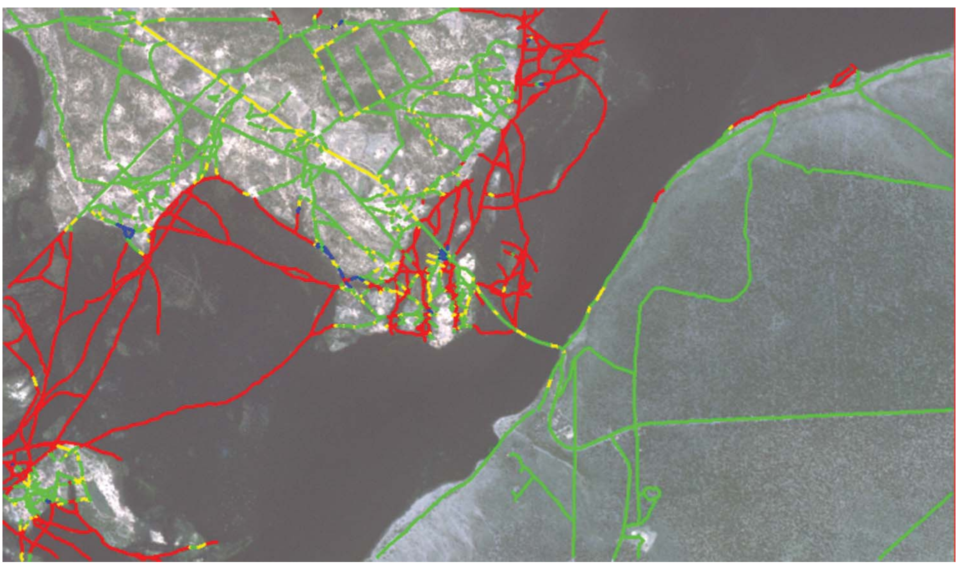

Figure 11. Result of the assessment system using all available input data (Chobe scenario) image t_1, image t_2, DEM and manual generated reference at time t_1; green = *trafficable*, yellow = *possibly flooded*, red = *flooded*, dark blue = *trafficable* (change: *flooded* → *trafficable*).

are very sensitive to this parameter s_1. So far the threshold value has to be adjusted manually. Further research is necessary in order to carry out an automatic parameter estimation.

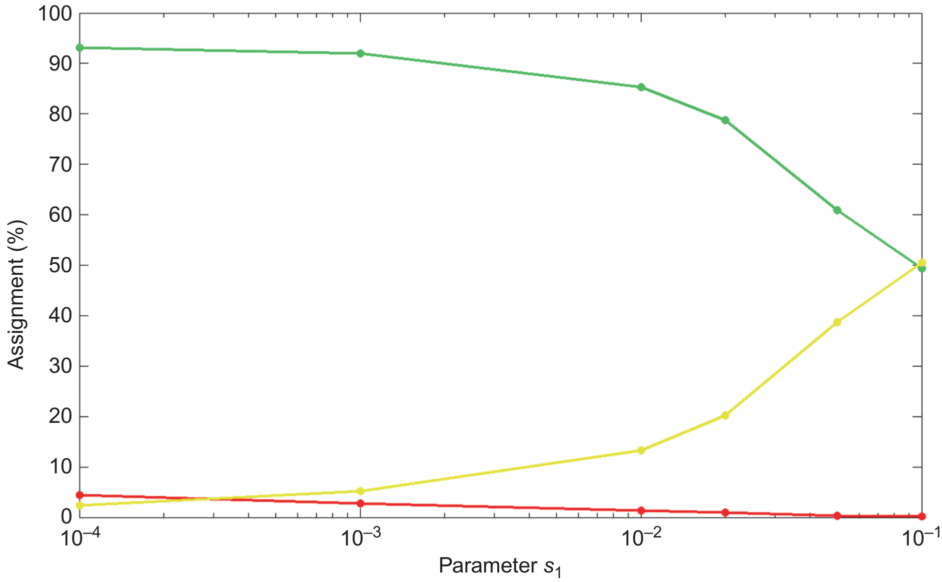

Figure 12. Performance of the system using different parameters s_1: green = 'correct assignment', yellow = 'manual control necessary', red = 'wrong assignment'.

5. Conclusion

In this article, a general framework of an assessment system of infrastructural objects and the benefit of the included data fusion on a probability level is shown. The improvement of the results by exploiting additional available data is demonstrated in two different test scenarios. The integration of multi-temporal imagery leads to an improvement of the assessment system concerning the correctness of the assessed objects and concerning the additional temporal information. Combining this basis with a rule-based approach, which is strongly dependent on the type of natural disaster and available input data, leads to very promising results with a very small rate of 'wrong assignments'.

In future work, the generic system will be tested on more scenarios with different sensors. In particular, the combination of optical images and SAR data should be investigated in more detail to derive statements on the benefit of these different kinds of sensors. In addition to the radiometric exploitation of the optical imagery, geometric features should be introduced as additional evidence of destructions, because man-made infrastructure objects can be represented, particularly those with geometric features. The combination of probabilities which are embedded into a rule-based workflow should be substituted using a general statistical framework. A promising theory for the combination of the probabilities is the model of dynamic Bayesian networks.

Acknowledgements

This work is part of the IGSSE project 'SafeEarth' funded by the Excellence Initiative of the German federal and state governments, and part of the project 'DeSecure' funded by the Federal Ministry of Economics and Technology.

References

Balz, T., Perissin, D., Soergel, U., Zhang, L. and Liao, M., 2009, Post-seismic infrastructure damage assessment using high-resolution SAR satellite data. In *Proceedings of the 2nd International Conference on Earth Observation for Global Changes (EOGC)*, Q. Tong and D. Li (Eds.), Chengdu, China, pp. 912–922.

Bamler, R., Reinartz, P., Riedlinger, T. and Schroeder, M., 2006, Moderne Raumfahrttechniken für Prävention bei Naturkatastrophen und das Krisenmanagement. In *Proceedings Symposium Future Security*, 2006, F. Gesellschaft (Ed.), Karlsruhe, Germany.

Bouguila, N. and Ziou, D., 2006, Unsupervised selection of a finite Dirichlet Mixture Model: an MML-based approach. *IEEE Transactions on Knowledge and Data Engineering*, **18**, pp. 993–1009.

Brivio, P., Colombo, R., Maggi, M. and Tomasoni, R., 2002, Integration of remote sensing data and GIS for accurate mapping of flooded areas. *International Journal of Remote Sensing*, **23**, pp. 429–441.

Butenuth, M., Gösseln, G., Tiedge, M., Heipke, C., Lipeck, U. and Sester, M., 2007, Integration of heterogeneous geospatial data in a federated database, ISPRS. *Journal of Photogrammetry and Remote Sensing*, **62**, pp. 328–346.

Canty, M. and Nielsen, A., 2006, Visualization and unsupervised classification of changes in multispectral satellite imagery. *International Journal of Remote Sensing*, **27**, pp. 3961–3975.

Chesnel, A.-L., Binet, R. and Wald, L., 2007, Quantitative assessment of building damage in urban area using very high resolution images. In *IEEE Urban Remote Sensing Joint Event*, 11–13 April 2007, IEEE (Eds.), Paris, France, pp. 1–5.

Coppin, P., Jonckheere, I., Nackaerts, K., Muys, B. and Lambin, E., 2004, Digital change detection methods in ecosystem monitoring: a review. *International Journal of Remote Sensing*, **25**, pp. 1565–1596.

Figueiredo, M. and Jain, A., 2002, Unsupervised learning of finite mixture models. *IEEE Transactions on Pattern Analysis and Machine Intelligence*, **24**, pp. 381–396.

Förstner, W., 1996, Pros and cons against performance characterization of vision algorithms. In *Proceedings of ECCV Workshop on Performance Characteristics of Vision Algorithms*, April 1996, H. Christensen, W. Förstner and C. Madsen (Eds.), Cambridge, UK, pp. 215–218.

Frey, D. and Butenuth, M., 2009, Classification system of GIS-objects using multisensorial imagery for near-realtime disaster management. *International Archives of Photogrammetry, Remote Sensing and Spatial Information Sciences*, **XXXVIII**(3/W4), pp. 103–108.

Gamba, P., Dell'Acqua, F. and Trianni, G., 2007, Rapid damage detection in the bam area using multitemporal SAR and exploiting ancillary data. *IEEE Transactions on Geoscience and Remote Sensing*, **45**, pp. 1582–1589.

Gerke, M. and Heipke, C., 2008, Image based quality assessment of road databases. *International Journal of Geoinformation Science*, **22**, pp. 871–894.

Guo, H.D., Lu, L.L., Ma, J.W., Pesaresi, M. and Yuan, F.Y., 2009, An improved automatic detection method for earthquake-collapsed buildings from ADS40 image. *Chinese Science Bulletin*, **54**, pp. 3303–3307.

Hotelling, H., 1936, Relations between two sets of variates. *Biometrika*, **28**, pp. 321–377.

Lu, D., Mausel, P., Brondizio, E. and Moran, E., 2004, Change detection techniques. *International Journal of Remote Sensing*, **25**, pp. 2365–2401.

Martinis, S., Twele, A. and Voigt, S., 2009, Towards operational near real-time flood detection using a split-based automatic thresholding procedure on high resolution TerraSAR-X data. *Natural Hazards and Earth System Science*, **9**, pp. 303–314.

MASON, D.C., SPECK, R., DEVEREUX, B., SCHUMANN, G., NEAL, J.C. and BATES, P.D., 2010, Flood detection in urban areas using TerraSAR-X. *IEEE Transactions on Geoscience and Remote Sensing*, **48**, pp. 882–894.

MCLACHLAN, G. and PEEL, D., 2000, *Finite Mixture Models* (New York: Wiley-Interscience).

MORAIN, S. and KRAFT, W., 2003, Transportation lifelines and hazards: overview of remote sensing products and results. *Proceedings of Remote Sensing for Transportation*, **29**, pp. 39–46.

NIELSEN, A., 2007, The regularized iteratively reweighted MAD method for change detection in multi- and hyperspectral data. *IEEE Transactions on Image Processing*, **16**, pp. 463–478.

NIELSEN, A., CONRADSEN, K. and SIMPSON, J., 1998, Multivariate alteration detection (MAD) and MAF postprocessing in multi-spectral, bitemporal image data: new approaches to change detection studies. *Remote Sensing of Environment*, **64**, pp. 1–19.

POHL, C. and VAN GENDEREN, J., 1998, Multisensor image fusion in remote sensing: concepts, methods and applications. *International Journal of Remote Sensing*, **19**, pp. 823–854.

REHOR, M., BÄHR, H., TARSHA-KURDI, F., LANDES, T. and GRUSSENMEYER, P., 2008, Contribution of two plane detection algorithms to recognition of intact and damaged buildings in lidar data. *The Photogrammetric Record*, **23**, pp. 441–456.

STRAMONDO, S., BIGNAMI, C., CHINI, M., PIERDICCA, N. and TERTULLIANI, A., 2006, Satellite radar and optical remote sensing for earthquake damage detection: results from different case studies. *International Journal of Remote Sensing*, **27**, pp. 4433–4447.

VOIGT, S., KEMPER, T., RIEDLINGER, T., KIEFL, R., SCHOLTE, K. and MEHL, H., 2007, Satellite image analysis for disaster and crisis management support. *IEEE Transactions on Geoscience and Remote Sensing*, **45**, pp. 1520–1528.

WALLACE, C., 2005, *Statistical and Inductive Inference by Minimum Message Length* (Berlin: Springer-Verlag).

WANG, Y., COLBY, J. and MULCAHY, K., 2002, An efficient method for mapping flood extent in a coastal floodplain using Landsat TM and DEM data. *International Journal of Remote Sensing*, **23**, pp. 3681–3696.

ZHANG, J., 2010, Multi-source remote sensing data fusion: status and trends. *International Journal of Image and Data Fusion*, **1**, pp. 5–24.

ZIOU, D., BOUGUILA, N, ALLILI, M.S. and EL ZAART, A., 2009, Finite gamma mixture modeling using minimum message length inference: application to SAR image analysis. *International Journal of Remote Sensing*, **30**, pp. 771–792.